UNIVERSITY OF CALIFORNIA

Santa Barbara

A probabilistic approach to calculate lags between benthic $d^{18}O$ signals across Termination 1

A Thesis submitted in partial satisfaction of the

requirements for the degree Master of Science

in Earth Science

by

Devin Scott Rand

Committee in charge:

Professor Lorraine E. Lisiecki, Chair

Professor David W. Lea

Professor Syee Weldeab

December 2019

The thesis of Devin Scott Rand is approved.

_____

David W. Lea

_____

Syee Weldeab

_____

Lorraine E. Lisiecki, Committee Chair

September 2019

ACKNOWLEDGEMENTS

This thesis is dedicated to my family for their unconditional love and support, to Lori for the honesty and special times, and to Roxanne for taking me to the beach and sharing her toys. I would especially like to thank my advisor, Lorraine Lisiecki, for the patience she has demonstrated, and the time she has dedicated, toward helping me become a capable scientist. This work would not have been possible without our collaborators, Charles Lawrence and Taehee Lee, who never tire of explaining statistical concepts. I am also grateful for my committee members, David Lea and Syee Weldeab, for their constructive criticism and insightful conversations. Finally I would like to thank Peter Green and Timothy Cuellar for maintaining a productive and prestigious working environment.

ABSTRACT

A probabilistic approach to calculate lags between benthic $d^{18}O$ signals across Termination 1

by

Devin Scott Rand

Changes in the $\delta^{18}O$ of benthic foraminiferal calcite ($\delta^{18}O_b$) from ocean sediment cores have been assumed to be a globally synchronous signal and are often used as a stratigraphic marker. However, previous studies have identified temporal offsets ("lags") between $\delta^{18}O_b$ signals that both introduce age errors during stratigraphic alignment and offer an opportunity to better understand the ocean circulation changes that occurred during Termination 1 (T1). We present a novel method to quantify benthic $\delta^{18}O_b$ lags by subtracting a core's radiocarbon age model from its $\delta^{18}O_b$ age model. Bayesian software probabilistically constructs radiocarbon age models, $\delta^{18}O_b$ aligned age models, and a stack that serves as the target for $\delta^{18}O_b$ alignment. Age models and lags are reported with median values and 95% confidence bands. To evaluate the effectiveness of this technique, we calculate lags for a depth transect of 12 cores in the Brazil Margin and compare our results with the temporal offsets found by *Lund et al.* (2015). The technique yields a statistically significant lag between lower intermediate (1802 – 2296 m) and deep (2500 – 2296 m) cores from 20 – 10 ka BP with median values ranging from a maximum lag of 3.44 kyr (95% confidence interval (CI): 2.43-4.24 kyr) at 20 ka BP to a minimum lag of 1.51 kyr (95% CI: 0.66-2.42 kyr) at 12 ka BP. These results agree with the 2-3 kyr offset described by *Lund et al.* (2015).

Additionally, our method identifies a previously undescribed lag between upper intermediate (1105-1627 m) and lower intermediate (1802-2296 m) cores that is statistically significant from 20 – 15 ka BP with a maximum value of 2 kyr (95% CI: 0.97 – 2.98 kyr) at 20 ka BP.

TABLE OF CONTENTS

I. Introduction

The oxygen isotope ratio of benthic foraminiferal calcite ($\delta^{18}O_b$) from ocean sediment cores is a proxy for changes in global ice volume, local water temperature, and salinity. Although previous studies have assumed that changes in benthic $\delta^{18}O_b$ are globally synchronous (**Imbrie et al., 1984**), recent studies have observed temporal offsets ("lags") of up to 4 kyr between some benthic $\delta^{18}O_b$ records during the Termination 1 (T1; 19-11.7 ka BP, **Skinner & Shackleton, 2005; Stern & Lisiecki, 2014**). Such unexpectedly large lags suggest a poor understanding of deep ocean circulation changes that occurred during this time. However, no study has developed a method to calculate the statistical significance with which these lags occur, nor have they been extensively and thoroughly mapped.

Measuring the frequency, magnitude, and statistical significance with which lags relative to a reference record occur is necessary for estimating the uncertainty of $\delta^{18}O_b$ age models and the implications of benthic $\delta^{18}O_b$ lags for reconstructions of deglacial ocean circulation change. Lag observations from previous studies are limited by their spatial coverage, lack of uncertainty estimates, and different measurement techniques which makes direct comparison difficult. Additionally, previous studies have not quantified changes in lags across the termination that could be indicative of the timing of changes in circulation or water mass properties (**Labeyrie et al., 2005; Lund et al., 2015; Skinner & Shackleton 2005; Stern & Lisiecki 2014; Waelbroeck et al., 2011**). We present a novel method that resolves these shortcomings by probabilistically measuring $\delta^{18}O_b$ lags as a function of time in individual sediment cores. The technique will facilitate mapping the occurrence of statistically significant lags throughout the ocean, which could provide an additional constraint for ocean circulation models to help reconstruct past water mass geometries (e.g.,

Gebbie, 2014; Gebbie et al., 2015). Furthermore, mapping the spatial distribution of these lags could assist with the selection of which cores to align for regional stacks or age model construction.

Our strategy for assessing benthic $\delta^{18}O_b$ lags as a function of time in individual sediment cores is to subtract the core's radiocarbon age model from one based on an assumption of synchronous $\delta^{18}O_b$ change with an alignment target. Furthermore, because both radiocarbon and $\delta^{18}O_b$-aligned age models have 95% confidence bands (**Lee et al., in preparation**), each lag calculation includes uncertainty estimates. We calculate lags for a depth transect of twelve cores from the Brazil Margin between 440-3924 m and compare our results with previously described temporal offsets (**Lund et al., 2015**). We evaluate whether the apparent pattern of lags is replicated and found to be statistically significant.

II. Background

2.1. Benthic $\delta^{18}O_b$ lag definition

Local changes in water mass properties are not necessarily synchronous with changes in global ice volume (**Riveiros et al., 2010; Cortese et al., 2007; Mashiotta et al., 1999; Shackleton, 2000**). While termination events are defined by the timing and pace of changes in global ice volume, benthic $\delta^{18}O_b$ records reflect the local $\delta^{18}O$ of seawater ($\delta^{18}O_{sw}$) and water temperature at the sea floor. The $\delta^{18}O_b$ value recorded at a given core site can change when the $\delta^{18}O_{sw}$ or temperature of end-member water masses change or when the boundary between two water masses shifts across a core site. Water mass properties of Northern Component Water (NCW) and Southern Component Water (SCW) likely changed diachronously due to bipolar seesaw events (**Schmittner et al., 2003; Shakun et al., 2012; Toggweiler & Lea, 2010**). For example, northern hemisphere cooling during Heinrich Stadial 1 (HS1, 17.5-14.7 ka BP) and the Younger Dryas (YD, 12.8-11.7 ka BP) occurred while temperatures in Antarctica increased (**Barker 2009; Epica, C.M., 2006**). Models suggest that these anti-phased hemispheric responses are likely associated with changes in AMOC (e.g., **He et al., 2013**); thus, the bipolar seesaw may not only produce differences in the timing of NCW and SCW deep water temperature change but also transit times and deep water mass boundaries.

Lags have previously been described when identifiable features (e.g., T1 onset) were recorded by $\delta^{18}O_b$ at different times between sites. However, lags can also reflect the extent to which $\delta^{18}O_b$ age models are incorrect. For example, assuming synchronous $\delta^{18}O_b$ change

by aligning a record with a T1 onset 15 ka BP to a different core with a T1 onset 18 ka BP would result in an age error of ~3 kyr, which would indicate a 3 kyr lag between two sites.

2.2. Potential causes of lags

One factor that affects the timings of benthic $\delta^{18}O_b$ change in different oceanic sites is the transit time of $\delta^{18}O$-depleted meltwater from the surface to the deep core site. Several authors (**Broecker et al., 1988; Duplessy et al., 1991; Gebbie & Huybers 2012; Keigwin et al., 1992; Mix & Ruddiman 1984; Shackleton et al., 1988; Skinner & Shackleton 2004; Skinner et al., 2010**) suggest, however, that glacial transit times in the deep North Pacific and Indian oceans are not large enough to explain the 4 kyr lags observed between ocean basins (**Skinner & Shackleton 2005; Stern & Lisiecki 2014**) and 2-3 kyr lags observed within the Atlantic (**Lund et al., 2015; Waelbroeck et al., 2011**). Therefore, asynchronous changes in water mass properties and/or boundaries during the LGM and T1 likely also contributed to these lags. For example, a model using modern-day circulation patterns demonstrated that a 4 kyr lag between the Pacific and the Atlantic may be caused by the early North Atlantic $\delta^{18}O_{sw}$ decrease compared with the later Antarctic isotope maxima early in T1 (**Gebbie, 2012**). The pace that meltwater enters the ocean affects its arrival to the ocean's interior (**Primeau & Deleersnijder, 2008; Gebbie & Huybers 2012**), and early Northern Hemisphere ice loss may have caused meltwater to reach the ocean's interior before meltwater from the southern hemisphere (**EPICA, C.M., 2006**).

The millennial-scale events that occurred during T1 are manifested in transient water mass geometry and ocean circulation changes. Northern hemisphere cold events (Heinrich Stadial 1 and the Younger Dryas) are characterized by a weakening of the Atlantic Meridional Overturning Circulation (AMOC), shoaling of North Atlantic Deep Water

(NADW), and vertical and latitudinal expansion of Antarctic Bottom Water (AABW), as indicated by measurements of ^{231}Pa/Th (**McManus et al., 2004**), Cd/Ca (**Marchitto & Broecker, 2006; Makou et al., 2010**), Δ^{14}C (**Skinner et al., 2010**), and δ^{13}C (**Curry & Oppo, 2005**). During the LGM, NADW may have shoaled above 2 km (referred to as Glacial North Atlantic Intermediate Water) while AABW occupied depths as shallow as 2.5 km at the Brazil Margin (**Boyle & Keigwin, 1987; Duplessey et al., 1988; Curry & Oppo, 2005; Marchitto & Broecker, 2006**). Additionally, the northern extent of Antarctic Intermediate Water (AAIW) may have expanded north (**Pahnke et al., 2008; Rickaby & Elderfield, 2005; Thornalley et al., 2011**) or receded south (**Came et al., 2008; Huang et al., 2014; Xie et al., 2012**) during HS1 and the YD. As water mass boundaries shift across core sites, these sites have the potential to experience asynchronous changes in local temperature or $\delta^{18}O_{sw}$.

Changes in water mass properties during the LGM and T1 may also have contributed to $\delta^{18}O_b$ lags across T1 (**Zhang et al., 2017**). Today, AABW has a lower salinity and potential temperature than NADW, which yields very similar $\delta^{18}O_b$ values throughout the deep Atlantic (**Adkins et al., 2002**). However, pore fluid measurements indicate that the total $\delta^{18}O_b$ change from the LGM to the Holocene in the North Atlantic was 1.9 ‰ - 2.0 ‰ while the change in the South Atlantic was 1.6 ‰ - 1.7 ‰ (**Adkins et al., 2002**). Therefore, NCW and SCW most likely had different water mass properties during the LGM and T1 (**Friedrich & Timmermann, 2012; Lynch-Stieglitz et al., 2007; Oppo et al., 2015**). The occurrence and timing of a core's transition from one water mass to another would affect its $\delta^{18}O_b$ signal.

2.3. Previous lag measurements

Multiple studies have identified lags between cores and stacks from different ocean basins. A lag between one core from the deep equatorial Pacific and one core from the deep North Atlantic (**Skinner & Shackleton, 2005**) was measured by placing each core on an independent radiocarbon age model (supplemented with SST alignments) and locating the mid-point of $\delta^{18}O_b$ change in each core based on 5-point smoothed signals. The Atlantic core was observed to record the T1-midpoint 3.9 kyr before the Pacific core. Subsequently, lags were measured in a compilation of seven cores on radiocarbon age models from the Atlantic, Pacific, and Indian Ocean basins by comparing peaks in the time derivative of $\delta^{18}O_b$. Deep water records were observed to lag intermediate water records by 1.5 kyr during HS1 and YD (**Labeyrie et al., 2005**).

An alternative approach is to establish average lags between regions using stacks. One study assumed regions of synchronous change and constructed seven stacks, combining the radiocarbon data from each region to construct age models (**Stern & Lisiecki, 2014**). During T1, the average lag between the Deep Pacific stack and the Deep North Atlantic stack was 1 kyr, with a maximum value of 1.7 kyr during the T1 midpoint. Although Stern & Lisiecki (2014) observed a smaller deep Pacific $\delta^{18}O_b$ lag than Skinner & Shackleton (2005), they found a 4 kyr lag for the onset of T1 between the Intermediate South Atlantic and Deep Indian stacks.

Lags have also been observed within the Atlantic basin during T1. A compilation of nine individual Atlantic cores on radiocarbon age models found that intermediate depth cores recorded the T1 onset 0.5 kyr before a deep North Atlantic core and 1.5 kyr before a deep South Atlantic core (**Waelbroeck et al., 2011**). Additionally, this study observed that

benthic $\delta^{18}O_b$ from the deep North Atlantic core decreased by 0.6 ‰ from 17-15 ka BP while the deep South Atlantic record only decreased by 0.2 ‰. A depth transect of twelve cores from the Brazil Margin found that intermediate cores (1802-2296 m) recorded a benthic $\delta^{18}O_b$ decrease 2-3 kyr before deep cores (2500-2951 m, **Lund et al., 2015**). In regional stacks constructed using a depth boundary of 2000 m, the Intermediate South Atlantic stack recorded the T1 onset 1 kyr before Intermediate North Atlantic, Deep North Atlantic, and Deep South Atlantic stacks (**Stern & Lisiecki, 2014**).

Each study used different criteria to identify lags based on the T1 onset (or midpoint), which may affect the inferred/reconstructed lag. One study calculated the mean $\delta^{18}O_b$ value from 20-17 ka BP and defined the beginning of T1 as the first point less than one standard deviation from the mean (**Waelbroeck et al., 2011**). Another study identified the T1 onset as the first point in each stack less than 0.1 ‰ of the maximum $\delta^{18}O_b$ value (**Stern & Lisiecki, 2014**). A third study provided approximate timings when $\delta^{18}O_b$ in each core began to change (**Lund et al., 2015**). In addition, the differences between results may also be caused by limited spatial coverage: i.e., lag measurements may reflect localized rather than basin-wide responses. For example, diachronous benthic $\delta^{18}O_b$ may exist within the regions defined by Stern & Lisiecki (2014). Lag patterns established on consistent criteria for a basin-wide compilation of individual cores would be helpful to better characterize the occurrence of lags and their implications for past circulation change.

III. Bayesian Lag Calculation Method

3.1. Application of Bayes' Theorem

We use Bayesian software (**Lee et al., in preparation**) to construct radiocarbon age models, $\delta^{18}O_b$ age models, and a target stack for $\delta^{18}O_b$ alignment. The software can be run in three different modes: ^{14}C-only, $\delta^{18}O_b$-only, and "dual proxy" in which both radiocarbon and $\delta^{18}O_b$ data are used to make age inferences. Our radiocarbon and $\delta^{18}O_b$-aligned age models used to calculate $\delta^{18}O_b$ lags are constructed in ^{14}C-only and $\delta^{18}O_b$-only modes, respectively. The Atlantic stack used for our $\delta^{18}O_b$ alignment target is constructed using dual proxy mode.

For each software mode, age uncertainty is estimated based on the distribution of 1000 Monte Carlo age model samples drawn in proportion to their posterior probabilities given the data. The probability of each age model sample depends on the modeled sedimentation rates as well as the fit to the radiocarbon data and/or $\delta^{18}O_b$ alignment target. The probability of any sampled age model is calculated using Bayes' theorem (Equation 1).

$$P(A_i|data,\theta,\phi) = \frac{P(data|A_i,\theta)P(A_i|\phi)}{\int P(data|A_i,\theta)P(A_i|\phi)dA_i} \quad (1)$$

In the above equation, A_i refers to the i^{th} age model sample, and the integration in the denominator is over all possible samples. The first term in the numerator, $P(data|A_i,\theta)$ is called the emission model. It calculates the probability of observing the residual between a given sample and the data (either the radiocarbon or $\delta^{18}O_b$). θ represents the model parameters related to the measurement uncertainties and intra-core variability in radiocarbon

and $\delta^{18}O_b$ data. The next term in the numerator, $P(A_i|\phi)$, is called the transition model and returns the probability of the particular set of sedimentation rates and changes that take place within an age model. The transition probability depends on model parameters, ϕ, that describe expected sedimentation rate variability, independent of the core's radiocarbon and $\delta^{18}O_b$ data. The product of the emission model and the transition model is normalized by dividing by the integral over these probabilities for every alignment (the denominator in Equation 1). The right-hand side of the equation returns the posterior probability of an age model sample given the data, the emission model parameters, and the transition model parameters.

3.2. Transition Model

The transition model is fundamentally based on a gamma distribution fit to the observed sedimentation rate changes of 37 cores on radiocarbon age models. Although this is the same compilation of sedimentation rates used by Lin et al. (2014), that study fit a mixture log-Gaussian distribution to the data. Here, we use a gamma distribution that better fits the observations. Because the gamma function has thicker tails, it allows for more variability in sedimentation rates.

The sedimentation rate at a given depth is dependent on the sedimentation rate at the previous depth. However, the algorithm would take too long to consider all possible pairs of sequential sedimentation rates allowed by the gamma distribution. Therefore, the previous sedimentation rate is split into three states: expansion, contraction, and average which represent sedimentation rates below, above or approximately equal to the mean sedimentation rate of the core. The compilation of observed sedimentation rates in 37 cores

(**Lin et al., 2014**) is used to estimate the frequency at which transitions between these three states occur whereas the gamma distribution describes the probability of different sedimentation rates within each state.

The software has three modes to calculate the probabilities of transitions between sedimentation rate states: fixed, local, and global. If the mode is set to fixed, the probabilities for transitions between states are calculated from the 37 cores used to fit the gamma distribution, and they remain constant during the run. If the mode is set to local, state transition probabilities are iteratively learned from the sedimentation rate changes of age model samples in individual input cores. If the mode is set to global, probabilities are iteratively learned considering age model samples from all input cores. We construct age models in the local mode and the target stack is in the global mode.

Some previously published age model construction algorithms base sedimentation rate change probabilities on user-specified tuning parameters (e.g., **Blaauw & Christen, 2011; Lougheed & Brachta, 2019**). The values of these parameters have the potential to significantly affect the median age model and 95% confidence width. Because sedimentation rate change probabilities in Lee et al. (**in preparation**) are based on previous observations, the constructed age model is less subjective compared to those constructed by software with user-specified tuning parameters.

3.3. Emission Model

The software uses different emission models to calculate the probability of radiocarbon and $\delta^{18}O_b$ residuals. The radiocarbon emission model calculates the probability of observing age offsets from radiocarbon ages and is the same model used in the Bayesian modeling software Bacon (**Blaauw & Christen, 2011**). The shape of the radiocarbon PDF

depends on the radiocarbon measurement uncertainty, reservoir age uncertainty, and the radiocarbon calibration curve.

The $\delta^{18}O_b$ emission model is a Gaussian distribution that returns the probability of observing a $\delta^{18}O_b$ residual between the input core and target under the assumption that the $\delta^{18}O_b$ records of the input and target are synchronous. Defining the Gaussian emission requires specifying the mean and variance of $\delta^{18}O_b$ as a function of time, which serves as an alignment target. That target variance should represent the expected $\delta^{18}O_b$ variability for the set of cores to be aligned. The variance of the target can affect both the median value and uncertainty of $\delta^{18}O_b$ age models. A larger target variance allows for more misfit between the $\delta^{18}O_b$ records.

3.4. Target stack

By combining data from multiple cores, stacks can be representative of changes in mean $\delta^{18}O_b$ within an ocean basin or region and are therefore more appropriate alignment targets than an individual $\delta^{18}O_b$ record from one core. Stacks also provide a way to measure $\delta^{18}O_b$ variance through time. Because the emission model should reflect $\delta^{18}O_b$ variance among the cores to be aligned, we create a target stack whose standard deviation reflects the average $\delta^{18}O_b$ variance in the Atlantic Ocean. This is accomplished by selecting input cores distributed throughout the low- and mid-latitude Atlantic: two cores from the Iberian margin, three cores from the northeast coast of Africa, one core from the Brazil Margin, and one core from the Ceara Rise (Figure 1). These cores span a depth range of 1268 – 3528 m. Resolving lags also depends on the temporal resolution of the $\delta^{18}O_b$ alignment target, thus another selection criterion is high resolution radiocarbon and $\delta^{18}O_b$ data. Each core in our

target stack has 8-28 radiocarbon ages and a $\delta^{18}O_b$ sample spacing between 100-400 years (Table 1).

Age inferences for stack construction are dual proxy, meaning that both radiocarbon ages and $\delta^{18}O_b$ alignments are used to construct age models for each core (**Lee et al., in preparation**). The $\delta^{18}O_b$ data assist age model construction before and after the last radiocarbon age and reduce age model uncertainty between radiocarbon measurements. Additionally, fewer cores are required to form a dual proxy stack than previous $\delta^{18}O_b$ -only stacking software (**Ahn et al., 2017; Lee et al., in preparation**). The near 1:1 agreement between dual proxy ages of each core in the stack and their respective ^{14}C-only age models (Figure 2) indicates that the dual proxy age models are similar to radiocarbon-based age models. Between 0 – 50 ka BP the average 95% confidence width for the dual proxy age models of individual cores is 1.2 kyr, and the average $\delta^{18}O_b$ standard deviation of the stack is 0.12 ‰ (Figure 3). The stack's median value and standard deviation are estimated continuously using a Gaussian process regression model (**Rasmussen & Williams, 2006**); however, the software provides output samples in 100 year increments. The Gaussian process regression model requires the use of a kernel that affects the smoothness of the stack. Here we use the Ornstein-Uhlenbeck kernel (**Rasmussen and Williams, 2006**).

3.5. Lag Calculations

Lags and their uncertainties are calculated at a given depth by the subtracting radiocarbon age model samples from $\delta^{18}O_b$ age model samples. Before this calculation is performed, radiocarbon and $\delta^{18}O_b$ age model samples are linearly interpolated to common depths. We choose to interpolate age model samples to depths in which either radiocarbon or $\delta^{18}O_b$ age data exist. To avoid uncertainties associated with extrapolation, lag calculations

only exist at depths spanned by both radiocarbon and $\delta^{18}O_b$ data. This is repeated for 1000 pairs of radiocarbon and $\delta^{18}O_b$ age models to generate 1000 lag samples from which 95% confidence intervals are calculated. Therefore, the uncertainties from radiocarbon and $\delta^{18}O_b$ age models are incorporated in lag uncertainties. It should be noted that, because the distributions of radiocarbon and $\delta^{18}O_b$ age model samples are not Gaussian, the distributions of lag samples are also not Gaussian. Therefore, we report median lag values rather than mean values.

All calculated lags are relative to the target stack. A positive lag implies that corresponding $\delta^{18}O_b$ features (probabilistically and continuously identified by the alignment process) occurred later in the input core than the target, while a negative lag occurs when $\delta^{18}O_b$ features were recorded in the input core before the target stack. The relative lag between two cores is equal to the difference between their lag times and should be independent of the choice of alignment target.

IV. Brazil Margin Data

4.1. Core sites

The Brazil Margin provides a good test case for evaluating our lag calculation method. Past water mass geometries have been reconstructed with high spatial resolution (**Curry & Oppo 2005; Lund et al., 2015; Makou et al., 2010; Oppo et al., 2015; Tessin & Lund, 2013**) and cores with benthic $\delta^{18}O_b$ and radiocarbon data span depths from 440 m to 3924 m. In addition, we can evaluate the extent to which our lag results reproduce the qualitative observations of previous studies (**Lund et al., 2015**) and whether these lags are statistically significant. Because modern day transit times of all cores in the depth transect are thought to differ by less than approximately 500 years (**Devries & Primeau, 2011; Gebbie & Huybers 2012**), any lags of a larger magnitude must be a result of transit time changes, water mass boundary shifts, or localized changes in water mass properties.

We use twelve cores from 440-3924 m in the Brazil Margin depth transect analyzed by Lund et al. (2015). Under the present water mass geometry (Figure 4), one core is sampled from South Atlantic Mode Water (440 m), two cores are sampled from depths within AAIW (1105-1268 m), seven from NADW (1627-3589 m), and one from AABW (3924 m). A recent water-mass reconstruction indicates that the core of AAIW at the Brazil Margin was at a depth of approximately 1000 m during both the LGM and Holocene (**Oppo et al., 2019**).However, during the LGM, the water masses bathing some of the core sites may have been different. Inverse modeling has been used to generate four different LGM water mass reconstructions consistent with available $\delta^{18}O_b$ and $\delta^{13}C_b$ data and produce different depth estimates for the LGM boundary between AABW and NADW at the Brazil

Margin (**Gebbie, 2014; Gebbie et al., 2015**). The water mass reconstruction that differs most from the present day (**Gebbie, 2014**) suggests that during the LGM as many as seven cores were bathed by AABW (2082-3924 m), two cores (1627-1802 m) were bathed by NADW (Figure 4), and two cores were bathed by AAIW (1105-1268 m).

4.2. Brazil Margin radiocarbon

Radiocarbon ages for Brazil Margin cores were measured on the planktonic species *Globigerinoides ruber* and *Globigerinoides sacculifer* with 8-29 measurements per core (Table 1). In order to assess the extent to which our lag calculation method reproduces the temporal offsets observed in Lund et al. (2015), we aim construct probabilistic radiocarbon age models similar to the previously published ones. Therefore, we use the same reservoir ages and reservoir age standard deviations of 400 and 200 years that were used in Lund et al. (2015), we reject the same radiocarbon ages that were previously rejected, and we adjust the transition model parameters to allow for larger sedimentation rate changes.

Ten of the twelve Brazil Margin cores contain reversals in their planktonic radiocarbon dates, and reversed radiocarbon dates were rejected by the original authors (**Hoffman & Lund, 2012; Lund et al., 2015; Sortor & Lund 2011; Tessin & Lund 2013**). Age reversals were originally attributed to the effects of bioturbation based on isotopic analyses of benthic foraminifera and benthic radiocarbon measurements (**Sortor & Lund, 2011**), low planktonic $\delta^{18}O_b$ and high $CaCO_3$ measurements (**Lund et al., 2015**), and low benthic $\delta^{18}O_b$ values (**Tessin & Lund, 2013**). However, many of these reversals were observed across depth ranges of approximately 60 cm, too large to be caused by bioturbation. Possible alternative causes of extensive age reversals are turbidite deposits or

radiocarbon contamination. In addition, two ages with overlapping uncertainties were averaged in 14GGC (**Lund et al., 2015**), and an age requiring a large sedimentation rate was rejected in 30GGC **(Tessin & Lund, 2013)**. The Bayesian modeling software we use here (**Lee et al., in preparation**) includes a non-biased method to identify outlying radiocarbon ages (**Christen & Sergio, 2009**). However, many of our age models would differ from those presented in Lund et al., (2015) if every radiocarbon age was used during age model construction. Therefore, we reject the same radiocarbon ages that were previously rejected.

Previous age models were constructed by interpolating between radiocarbon ages and resulted in large sedimentation rate changes. To generate probabilistic radiocarbon age models similar to the ones previously used, we adjusted some of the default parameter settings in our probabilistic software. Specifically, we expanded the allowable normalized sedimentation rate changes to include ratios of 1:6 and 6:1 (compared to the standard ratio range of 1:4 to 4:1). In addition, a parameter describing the transition model (calculated by fitting the gamma distribution to observed sedimentation rate changes) was adjusted from 4.02 to 2, effectively widening the distribution and allowing for larger sedimentation rate changes. If turbidite flows at the Brazil Margin caused large sedimentation rate changes, then these parameter adjustments may be reasonable.

4.3. Brazil Margin $\delta^{18}O_b$

Benthic $\delta^{18}O_b$ for the Brazil margin cores are measured on *Cibicidoides wuellerstorfi, Cibicidoides spp.,* and *Planulina., spp.* with resolutions ranging from 126 to 1000 years on average between measurements. A species correction of 0.47‰ was applied to convert all measurements to the *Uvigerina* scale (**Marchitto et al., 2014**). However, this specific correction used does not affect the $\delta^{18}O_b$ alignments because the Bayesian software

applies an average shift and scale to better align input records to the target. Specifically, the software attempts to fit the $\delta^{18}O_b$ residuals between the input and target to a Gaussian distribution. One core has a particularly noisy $\delta^{18}O_b$ record (30GGC) while two other cores have relatively low resolution (63GGC and 125GGC). The quality of the alignments for these cores may suffer due to the low signal to noise ratio or low resolution (Figure 6).

In order to guide the $\delta^{18}O_b$ alignment process for the first and last data points, start and end ages from the previous radiocarbon age models (**Lund et al., 2015**) are input to the Bayesian software. The software treats these ages as an additional age constraint, analogous to radiocarbon dates, but specified as a uniform probability distribution with a total confidence width of 2 kyr. Because any age model sample that does not pass through the specified ages has a probability equal to zero, age models are forced to fall within the specified confidence intervals for the start and end ages of each core. This strict constraint may underestimate start and end uncertainty.

V. Results

5.1. Age model results

Radiocarbon and $\delta^{18}O_b$ age models for the twelve cores from the Brazil Margin are plotted in Figure 5. Dotted blue and red lines represent values of the radiocarbon and $\delta^{18}O_b$ age models, and the shaded regions display 95% confidence bands. Also shown are radiocarbon ages and their 95% confidence intervals converted to calendar years (horizontal black lines), the start and end ages for the $\delta^{18}O_b$ age models (horizontal pink lines), and the depth of each $\delta^{18}O_b$ measurement (red triangles on the y-axis). The solid black lines are the age models used by Lund et al. (2015).

To characterize the uncertainty of our age models, we calculate the mean width of 95% confidence intervals across a time window of 10 to 20 ka BP (Table 2). The average uncertainties for radiocarbon age models range from 0.66 kyr to 2.41 kyr, with a mean of 1.24 kyr across all cores. Average uncertainties for $\delta^{18}O_b$ age models are similar with a range from 0.52 kyr to 2.12 kyr and a mean of 1.26 kyr.

5.2. Lags

Lags are calculated as the difference between $\delta^{18}O_b$ and radiocarbon age models between 10-20 ka BP (Figure 7). The largest lags are observed in cores 30GGC and 125GGC with magnitudes of 3.8 and 4.0 kyr relative to the target stack. The largest leads are calculated for 36GGC and 42JPC with lags of approximately -1.3 and -1.4 kyr relative to the target stack.

The 95% confidence intervals of lags are calculated from the distribution of 1000 pairs of radiocarbon and $\delta^{18}O_b$ age model samples. A core's lag uncertainties are inherently larger than the uncertainties of its ^{14}C-only and $\delta^{18}O_b$-only age models. Average uncertainties from 10-20 ka BP range from 1.12 kyr to 3.12 kyr, with a mean of 1.86 kyr. Lags are deemed statistically significant when the zero line falls outside of the 95% confidence bands. Statistically significant lags are observed in every core except 33GGC and 22GGC.

VI. Comparison of Brazil Margin lags to Lund et al. (2015)

Figure 8 shows the Hovmöller diagram originally presented in Lund et al. (2015). The contours display the $\delta^{18}O_b$ departures from mean LGM values (defined from 19-23 ka BP) for each core. Before constructing the diagram, a 2 kyr smoothing was applied to each core. Based on these results, Lund et al. (2015) describes two "$\delta^{18}O$ delineated water mass boundaries." The first, is a 2-3 kyr temporal offset between intermediate cores (1802-2296 m) and deep cores (2500-2951) that persisted throughout the termination and is easily visible in the Hovmöller diagram. The second, located between 2951 m - 3589 m, is defined during HS1. If our results agree with these observations, the magnitude of the relative lag between intermediate and deep cores should agree with the magnitude of the offset described by Lund et al. (2015), and we should observe a lag between deep and abyssal cores during HS1. In addition, we evaluate whether the observed lags are statistically significant.

We create four depth groupings of cores based on the timing of the -0.2 ‰ $\delta^{18}O_b$ contour in the Hovmöller diagram. The four groups are defined as follows: upper intermediate (3 cores between 1105-1627 m), lower intermediate (three cores between 1802-2296 m), deep (three cores between 2500-2951 m), and abyss (two cores between 3589-2924 m). Differences between these groups are easily identifiable in Figure 9 which displays lag estimates as a function of depth in two kyr increments from 18-10 ka BP. Similar core groups were loosely defined in Lund et al. (2015) based on $\delta^{13}C$ observations in addition to $\delta^{18}O_b$ observations. However, they included 17JPC in the lower intermediate group based on its $\delta^{13}C_b$, whereas we place the core in the upper intermediate group based on the -0.2 ‰ $\delta^{18}O_b$ contour in Figure 8.

To quantify how our lag estimates compare with those depicted in the Hovmöller diagram (Figure 8), we average lags from individual cores within each of the four groups to create four lag stacks. Each lag stack consists of 1000 samples calculated as the mean of the individual lag samples from the 2-3 cores in that group. Median values and 95% confidence bands of each lag stack are defined by the distribution of the 1000 stack samples (Figure 10).

Differences between lag stacks are used to calculate relative lags, which are compared with the $\delta^{18}O_b$-delineated water mass boundaries identified by Lund et al., (2015). The advantage of calculating relative lags is that they should be independent of the choice of target stack used as the reference point for the original lag calculations. Specifically, we compare the magnitude and the statistical significance of the relative lags between neighboring stacks (Table 3) with the offsets and water mass boundaries that were previously identified.

The relative lag between the lower intermediate and deep stacks agree well with the observations of Lund et al., (2015). There is a statistically significant offset between the two groups ranging from 3.44 kyr (95% CI: 4.24-2.43 kyr) to 1.51 kyr (95% CI:2.42-0.66 kyr) across the entire termination. The magnitude of the relative lag decreases towards the end of the termination, in agreement with the Hovmöller diagram. The relative lag between the deep and abyssal stacks is statistically significant from 20-17 ka BP but disappears by 13 ka BP, despite the variability between these depths in the Hovmöller diagram at this time.

Although Lund et al. (2015) provides no comparison of the upper and lower intermediate depths, our lag calculation method finds a statistically significant lag from 20-15 ka BP, with a maximum value of 2.00 kyr (95% CI: 0.97 – 2.98 kyr) at 20 ka BP. Comparing the group lag stacks (Figure 10) reveals that the upper intermediate lag stack

abruptly decreases by approximately 1.5 - 2 kyr at 16 ka BP. Thus, the lag stacks reveal differences in the timing of $\delta^{18}O_b$ change between the upper intermediate and lower intermediate depths until approximately 15 ka BP that is difficult to detect in the Hovmöller diagram.

While the large-scale structure and temporal evolution of our results match that of the Hovmöller diagram (Figure 9), the lag estimates for core 63GGC (2732 m) differ in the first half of the termination. In the Hovmöller diagram, core 63GGC is the last core to reach the 0 ‰ contour and maintains a relatively positive value throughout the termination. However, in our lag time slices, 63GGC has a lag close to zero at 18 ka BP (the smallest lag in the deep group), and its lag does not become statistically significant until 14 ka BP. Figure 5 shows that this discrepancy arises from differences in the radiocarbon age models used. Despite increasing the number of sedimentation rate ratios used and changing the gamma function parameter of the transition model, the radiocarbon age model still does not pass through the center of the last two radiocarbon ages. Sensitivity tests should be conducted to investigate whether additional increases in sedimentation rate variability can resolve this discrepancy and whether such a change would significantly alter the estimated lags of the other cores.

Overall, our lag calculations agree well with the lags described in Lund et al. (2015). Lag calculations are found to be statistically significant where Lund et al. (2015) identified $\delta^{18}O$-delineated water mass boundaries, and the median lag magnitudes agree with the previously published estimates. Furthermore, our lag calculation method quantifies changes in lags during the termination. From 20 to 10 ka BP, the relative lag between the deep and abyss stacks decreased by approximately 2.6 kyr, and the relative lag between the lower

intermediate and deep stacks decreased by approximately 1.76 kyr. We also identify a statistically significant lag between the upper intermediate and lower intermediate stacks from 15-20 ka BP.

VII. Discussion

The magnitude and uncertainties of our lag calculations depends on the median values and uncertainty estimates of the radiocarbon and $\delta^{18}O_b$ age models. Changes to the model parameters and the standard deviation of the target stack have the potential to result in different age model median values and uncertainty widths. To address this, we plan to perform a series of sensitivity tests in which one model parameter is changed at a time and age model results are compared to the default value. Parameters we plan to test are the standard deviation of the target stack, the process in which sedimentation rates for individual cores are learned during age model construction, the allowed maximum and minimum sedimentation rate changes, and the parameters controlling the shape of the transition model.

Sedimentation rate change restrictions during age model construction result in lag estimates produced that are inherently autocorrelated. Thus, the ability of lags to respond rapid water mass property changes or rapid shifts in a water mass boundary is limited. Sensitivity tests could also be used to evaluate the timescales of variability that can be detected.

A statistically significant relative lag between two cores is ultimately caused by local differences in the $\delta^{18}O_b$ signals at those sites. Lags larger than differences in modern transit times could be indicative of transit time changes, asynchronous changes in water mass properties, or shifts in water mass boundaries. Although the statistically significant lags we calculate here may reveal past ocean circulation changes, they cannot be interpreted directly

as water mass tracers. Two cores that are bathed continuously by the same water mass should have matching patterns of lags, which could reflect the timing of water mass property change relative to a core bathed by a different water mass. However, relative lags can also be generated when a water mass boundary shifts across one core site but not the other. Therefore, comparison of observed lags with simulated lags from ocean circulation models is essential for the interpretation of water mass geometry changes using lag results.

Interpretation of the complex pattern of lags observed in the Brazil Margin would also benefit from comparison with other proxies and a wider spatial distribution of core sites (e.g., including those representing end-member water masses). Additionally, $\delta^{18}O_b$ lag data (and their uncertainties) could be compared with those predicted by different ocean circulation models.

Planned future work includes lag calculations across the Atlantic basin to help resolve the uncertain timings and locations of water mass boundary shifts during T1. For example, previous studies have used Cd/Ca paired with $\delta^{13}C$ measurements, $\delta^{13}C_{as,}$ (**Came et al., 2008; Makou et al., 2010; Rickaby & Elderfield, 2005**) and neodymium isotope measurements, ε_{Nd}, (**Howe et al., 2016; Huang et al., 2014; Pahnke et al., 2008; Xie et al., 2012**) to infer changes in the northern extent of AAIW during millennial scale events. However, there is disagreement as to whether AAIW expanded north or retreated south during HS1 and the YD.

A recent compilation of 92 Atlantic cores (**Waelbroeck et al., 2019**) on radiocarbon age models (for low latitude cores) and SST or magnetic age models (for high latitude cores) will provide a large collection of sites for basin-wide lag time calculations. In particular, new data from this compilation will increase the resolution of radiocarbon age models.

Additionally, the differences between our radiocarbon age models and the age models from this study may shed light on the differences between our dating methods.

VIII. Conclusion

We present a novel method to quantitatively measure the magnitudes and uncertainties of temporal offsets between $\delta^{18}O_b$ signals. By subtracting a core's radiocarbon age model from its $\delta^{18}O_b$ age model, we calculate time series of $\delta^{18}O_b$ lags. Age models are constructed with Bayesian software that combines the probabilities of observing the data-model misfit resulting from an age model with the sedimentation rate changes of that age model. A dual proxy stack constructed from the $\delta^{18}O_b$ and radiocarbon data of seven Atlantic cores serves as the target for $\delta^{18}O_b$ alignment. Lags are calculated relative to the target stack, and lag uncertainties are derived from radiocarbon and $\delta^{18}O_b$ alignment age uncertainties.

We use a transect of Brazil Margin data as a test case of our lag calculation method and compare our results with the qualitative lag descriptions of Lund et al. (2015). Lags from different depth ranges are averaged to create lag stacks, and the relative lags between lag stacks is shown to match the lag descriptions from Lund et al. (2015). Specifically, the 2-3 kyr offset between lower intermediate and deep cores is reflected in our results as a statistically significant lag from 20 – 10 ka BP with median values ranging from 3.44 kyr (95% CI: 4.24-2.43 kyr) at 20 ka BP to 1.51 kyr (95% CI:2.42-0.66 kyr) at 12 ka BP. The offset between deep and abyssal cores identified by Lund et al. (2015) is estimated to have a maximum relative lag of 2 kyr (95% CI: 0.97 – 2.98 kyr) at 20 ka BP. Our lag calculation method also reveals an additional offset from 20 – 15 ka BP between the upper intermediate and lower intermediate depths, which was not previously described and which is estimated to have a maximum relative lag of 2 kyr (95% CI: 0.97 – 2.98 kyr) at 20 ka BP.

This new probabilistic method for measuring lags demonstrates that statistically significant lags occur at the Brazil Margin that are larger than present day differences in transit times. These lags could result from a combination of changes in circulation transit times, water mass properties, and water mass boundaries during the LGM and T1. Applying this method to a large population of cores could help constrain past circulation changes through comparison with ocean circulation models.

IX. Figures

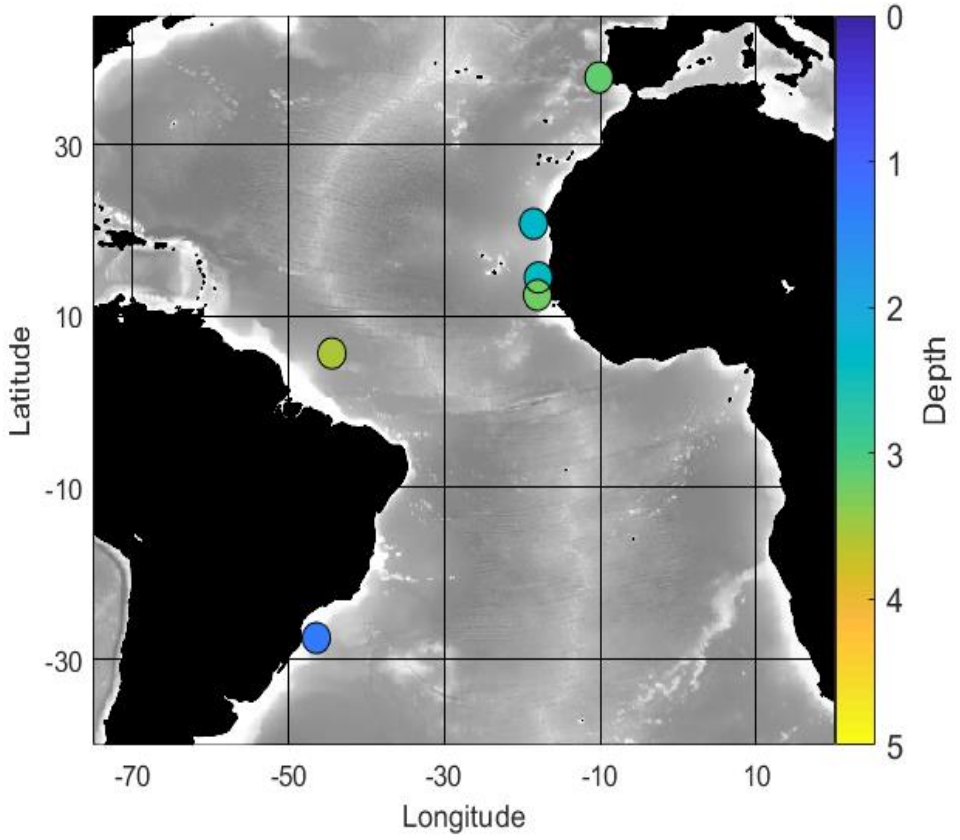

Figure 1: The locations of seven cores used to create the target stack. The large spatial distribution captures the variance of $\delta^{18}O_b$ in the Atlantic Ocean.

Core	Lat	Long	Depth	$\delta^{18}O_b$ res.	^{14}C ages	d.R	d.STD	Publication
EW9209-2JPC	5.6	-44.5	3528	330	11	400	200	Curry and Oppo [1997] , Curry et al. [1999]
GeoB7920-2	20.8	-18.6	2278	400	8	400	200	Tjallingii et al. [2008], Collins et al. [2011]
GeoB9508-5	14.5	-18	2384	170	12	400	200	Mulitza et al. [2008]
GeoB9526-5	12.4	-18.1	3223	370	8	400	200	Zarriess and Mackensen [2010, 2011], Zarriess et al. [2011]
KNR159-5-36GGC	-26.7	-46.5	441	116	8	400	200	Lund, 2015
MD95-2042	37.8	-10.2	3146	100	28	500	100	Shackleton et al. [2000, 2004]
MD99-2334	37.8	-10.2	3166	300	12	400	200	Skinner et al. [2003], Skinner and Shackleton [2004, 2005]

Table 1: The latitude longitude and depth (columns 1-3), $\delta^{18}O_b$ resolution (column 4), number of radiocarbon ages (column 5), radiocarbon reservoir age (column 6), radiocarbon reservoir age standard deviation (column 7), original publication (column 8).

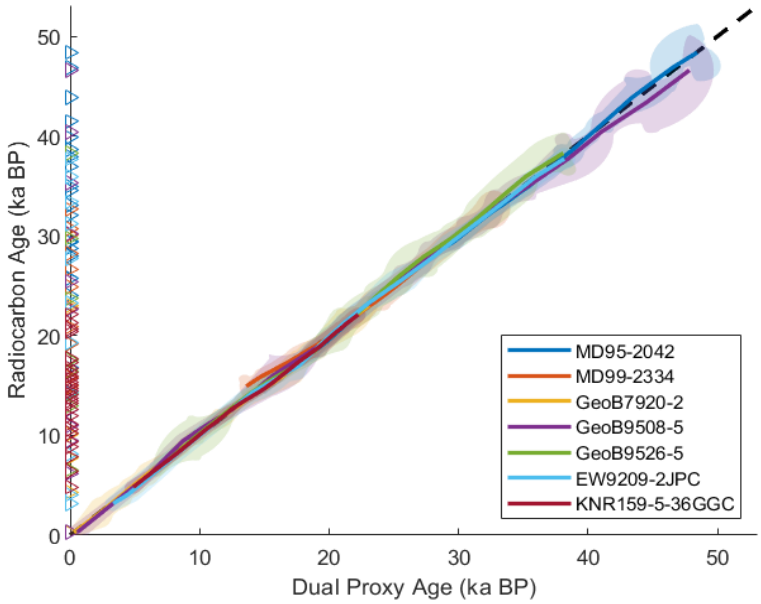

Figure 2: The dual proxy age vs. radiocarbon age for the seven cores in the target stack. Triangles on the y-axis indicate the calendar ages that radiocarbon ages exist for each core (color coded). Shaded regions indicate 95% confidence bands defined by the dual proxy and radiocarbon age model samples. Dual proxy ages are inferred from both radiocarbon and $\delta^{18}O_b$ data. Plots for each core lie close to the 1:1 line, demonstrating that dual proxy ages are similar to radiocarbon ages.

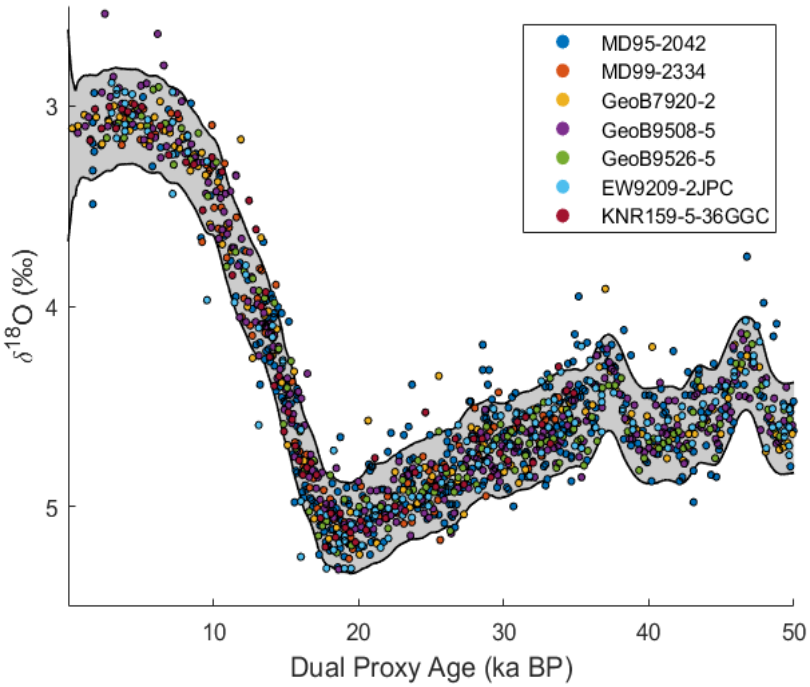

Figure 3: Individual $\delta^{18}O_b$ data points of the seven cores in the target stack. Grey shaded areas represent the stack's 2-sigma.

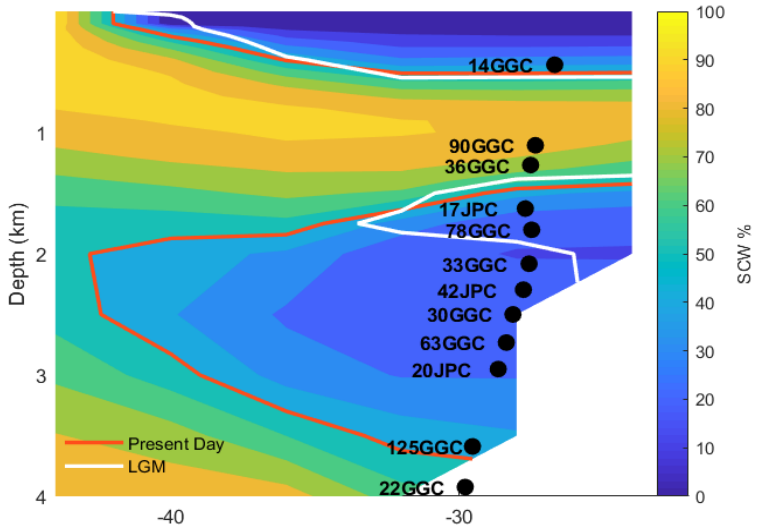

Figure 4: The Brazil Margin depth transect. The red and white contours represent the borders between northern component water and southern component water (SCW) for the present day and LGM, respectively. Borders are defined as the southern component water 50% contour. Southern component water is defined as water that was last at the surface in Antarctic and Subantarctic regions (**Gebbie & Huybers, 2010**). Contours are based on the present day 2012 reconstruction of Gebbie & Huybers (2012) and the LGM 2014ALT reconstruction of Gebbie (2014). The colored contours display the percentage of present-day southern component water. According to these reconstructions, six cores that were bathed by southern component water during the LGM, transitioned to northern component water during T1.

Core	Depth	$\delta^{18}O_c$ Uncertainty	$\delta^{18}O_b$ Resolution	^{14}C Uncertainty	# Ages	Lag Uncertainty
14GGC	441	1.11	357.14	1.93	4	2.28
90GGC	1105	0.78	312.5	1.25	5	1.47
36GGC	1268	1.4	416.67	0.83	19	1.67
17GGC	1627	1.13	185.19	1.4	6	1.84
78GGC	1802	0.86	126.58	0.66	12	1.12
33GGC	2082	0.96	217.39	0.92	11	1.38
42JPC	2296	0.52	135.14	1.02	7	1.19
30GGC	2500	1.87	434.78	1.23	4	2.39
63GGC	2732	1.2	555.56	1.2	4	1.7
20JPC	2951	1.83	1000	2.41	3	3.12
125GGC	3589	2.12	384.62	1.15	6	2.46
22GGC	3924	1.33	312.5	0.87	9	1.66
Average		1.26	369.84	1.24	7.5	1.86

Table 2: Average values of $\delta^{18}O_b$ uncertainty and resolution, and radiocarbon uncertainty and the number of ages between 10-20 ka BP. Core depth (column 2), average $\delta^{18}O_b$ age model 95% confidence width (column 3), average $\delta^{18}O_b$ resolution (column 4), average radiocarbon age model 95% confidence width (column 5), the number of radiocarbon ages (column 6), and the average 95% confidence width of estimated lags (column 7).

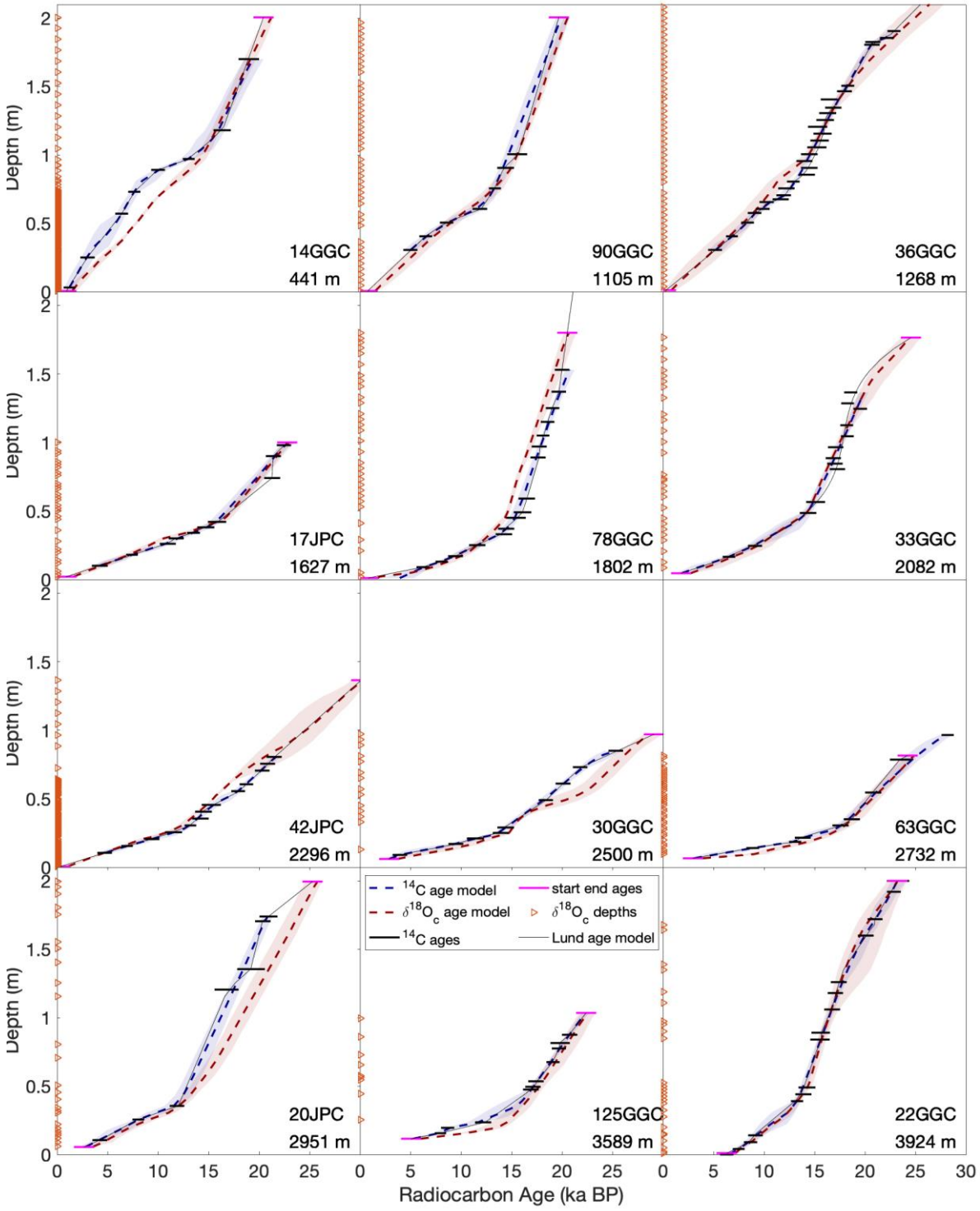

Figure 5: Radiocarbon (blue) and $\delta^{18}O_b$ (red) age models for the twelve Brazil Margin cores. Shaded regions are the 95% confidence bands, black horizontal lines are radiocarbon ages, and pink horizontal lines are the start and end ages from Lund et al., (2015). Traingles on the y-axis are the depths in which $\delta^{18}O_b$ data exist. Thin black lines are the age models presented in Lund et al., (2015).

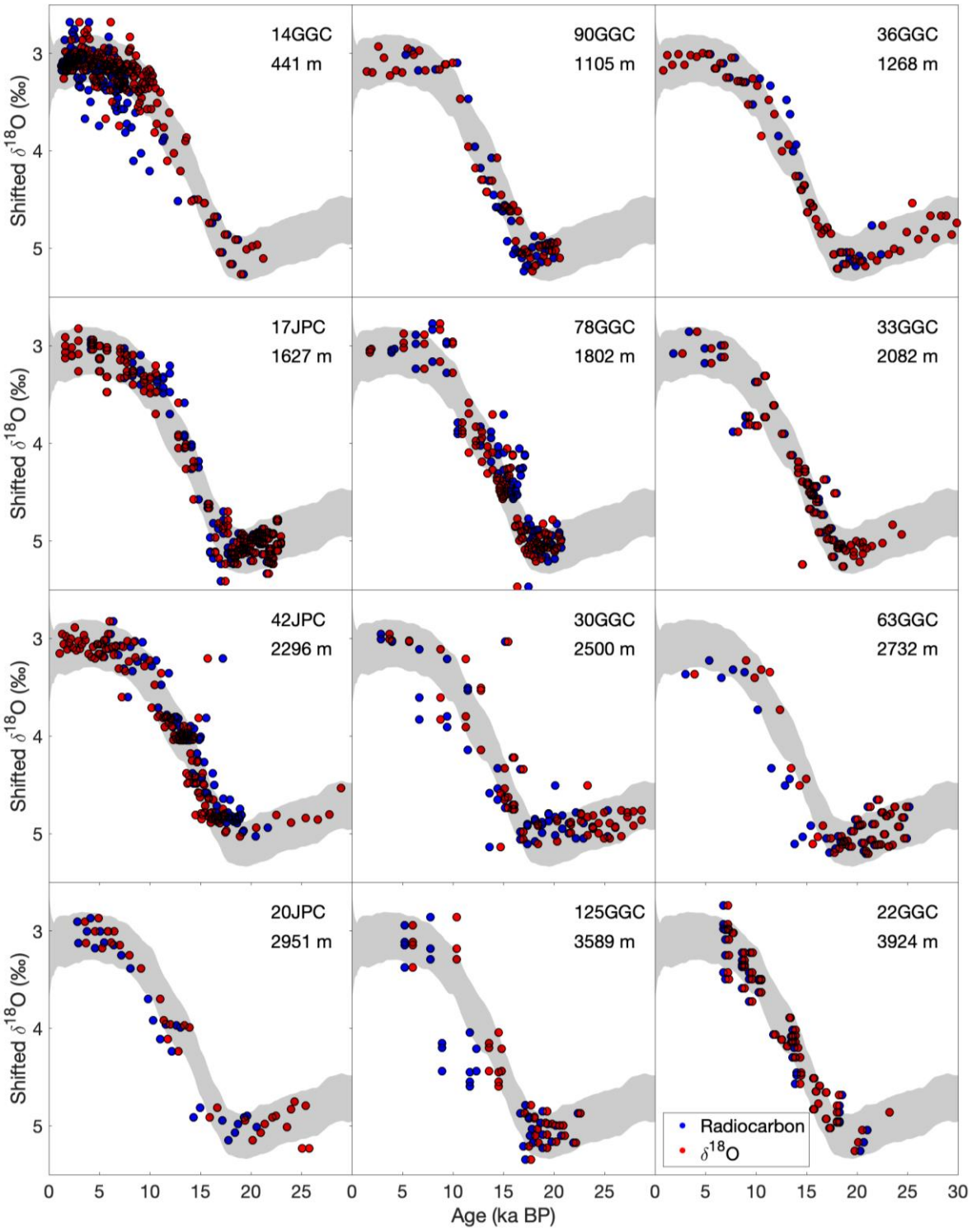

Figure 6: Shifted and scaled $\delta^{18}O_b$ for each Brazil Margin core on the radiocarbon age model (blue) and on the $\delta^{18}O_b$ age model (red). The 95% confidence interval of the Atlantic target stack is shown in gray

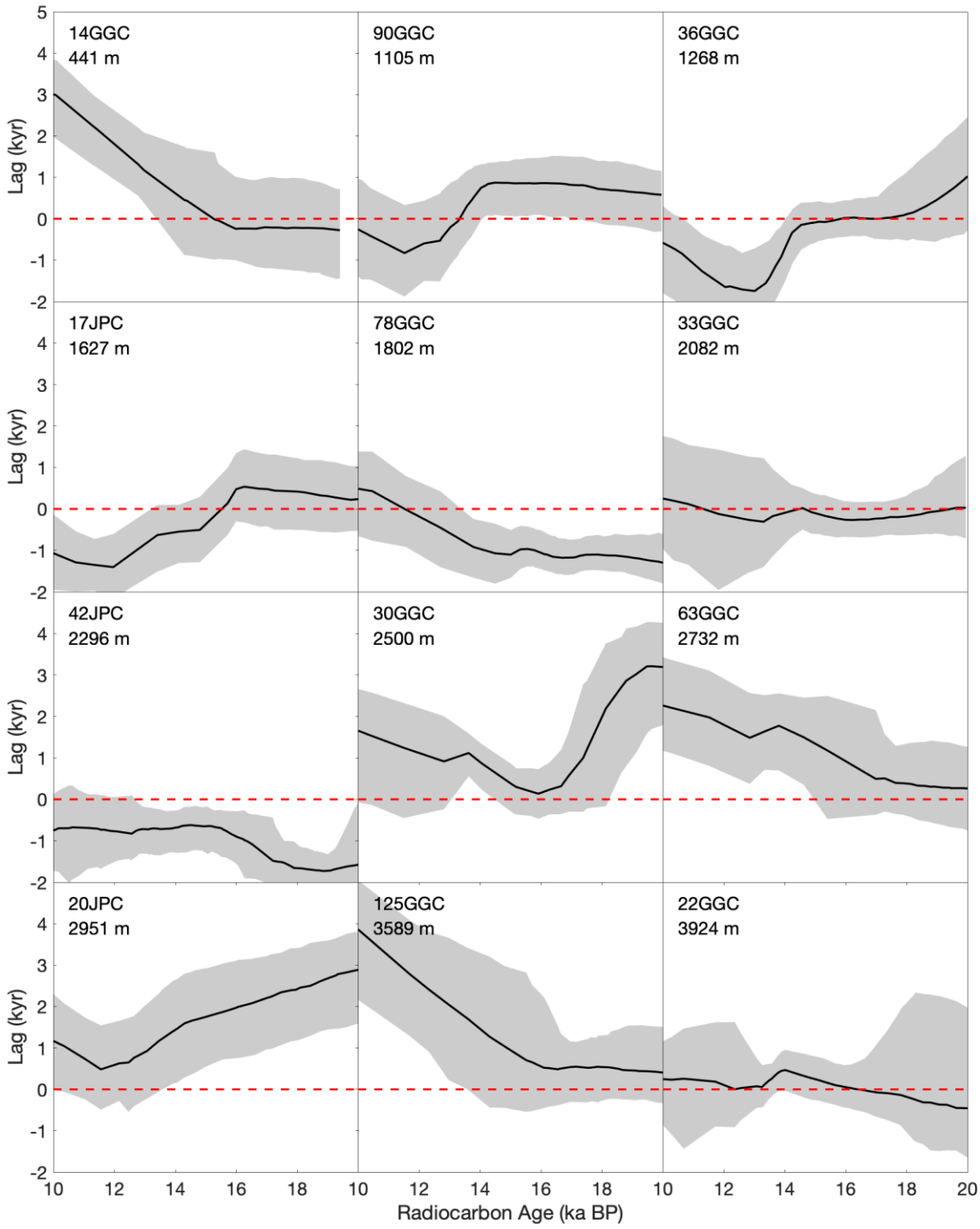

Figure 7: Lag times for the twelve Brazil Margin cores. Shaded regions are the 95% confidence widths, and black lines are medians values. The dotted red line is the zero line. A lag is deemed statistically significant when 95% confidence bands do not overlap the zero line.

Time (ka BP)	Upper-Lower (kyr)	Lower-Deep (kyr)	Deep-Abyss (kyr)
10	-0.64, (-1.48 - 0.23)	-1.68, (-2.65 - -0.71)	-0.64, (-1.41 - 0.72)
11	-0.86, (-1.71 - -0.06)	-1.55, (-2.43 - -0.60)	-0.86, (-1.40 - 0.79)
12	-0.84, (-1.72 – 0.00)	-1.51, (-2.42 - -0.66)	-0.84, (-1.39 - 0.78)
13	-0.40, (-1.16 - 0.25)	-1.64, (-2.39 - -0.78)	-0.40, (-0.95 - 1.08)
14	0.39, (-0.17 - 0.91)	-1.93, (-2.54 - -1.29)	0.39, (-0.70 - 1.41)
15	0.76, (0.28 - 1.26)	-1.75, (-2.44 - -1.08)	0.76, (-0.65 - 1.45)
16	1.19, (0.69 - 1.71)	-1.73, (-2.47 - -1.04)	1.19, (-0.28 - 1.5)
17	1.32, (0.80 - 1.88)	-2.05, (-2.78 - -1.31)	1.32, (0.01 - 1.78)
18	1.39, (0.85 - 1.97)	-2.54, (-3.27 - -1.67)	1.39, (-0.02 - 2.24)
19	1.44, (0.84 - 2.10)	-2.92, (-3.59 - -2.01)	1.44, (0.30 - 2.78)
20	2.00, (0.97 - 2.98)	-3.44, (-4.24 - -2.43)	2.00, (0.52 - 3.04)

Table 3: The relative lag at 1 kyr increments between 20-10 ka BP between the upper and lower stacks (column 1), the lower and deep stacks (column 2), and the deep and abyss stacks (column 3). 95% confidence bands for each time step are displayed in parentheses next to the median values.

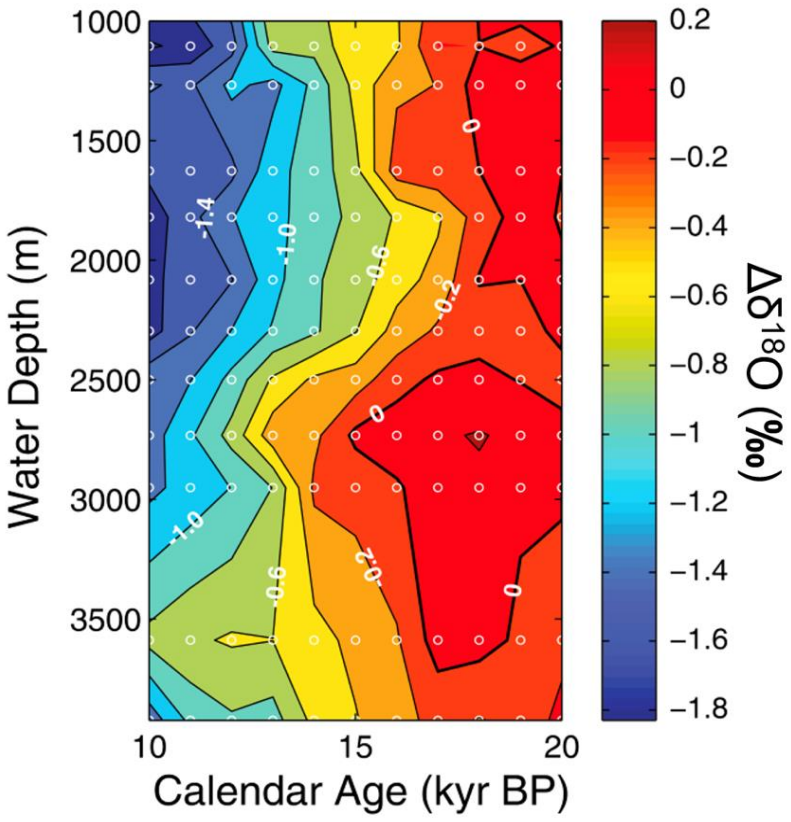

Figure 8: The Hovmöller diagram originally presented in Lund et al., (2015). Contours represent the $\delta^{18}O_c$ departure from the mean LGM value in each core. Reproduced with permission from Wiley Online Library ©2015. American Geophysical Union. All Rights Reserved

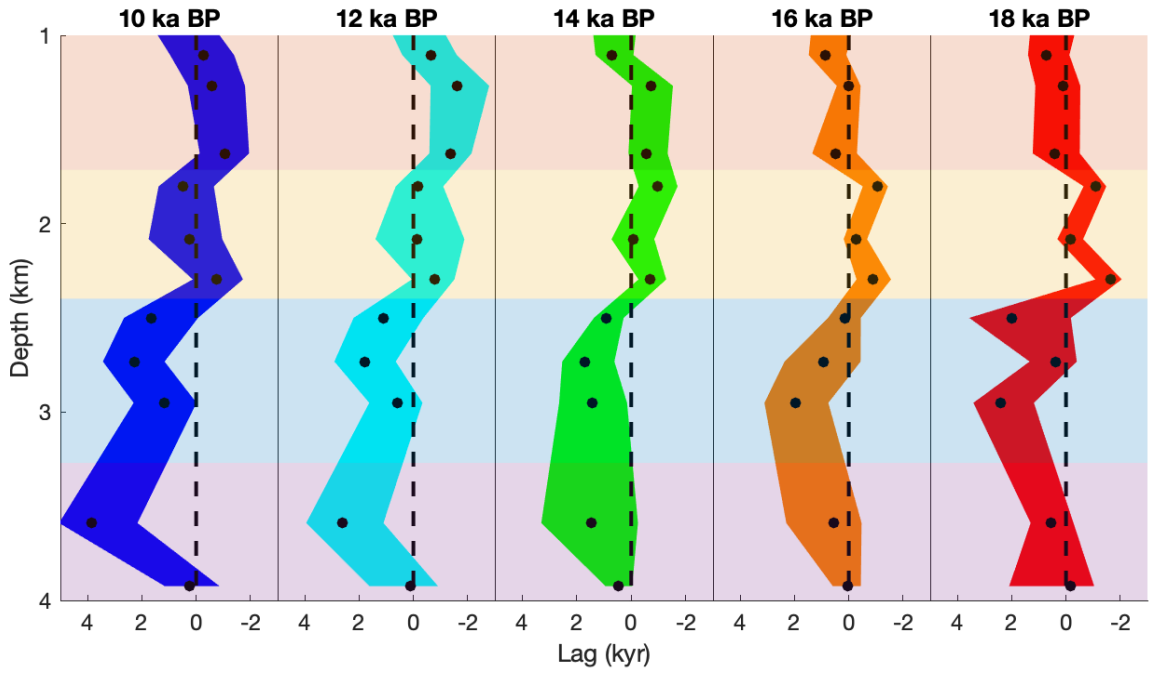

Figure 9: Lag time slices of the 12 Brazil Margin cores. The color of the 95% confidence band is aligned with Figure 8. The shaded colors show the upper intermediate (blue), the lower intermediate (red), the deep (yellow), and the abyss (purple) depth ranges.

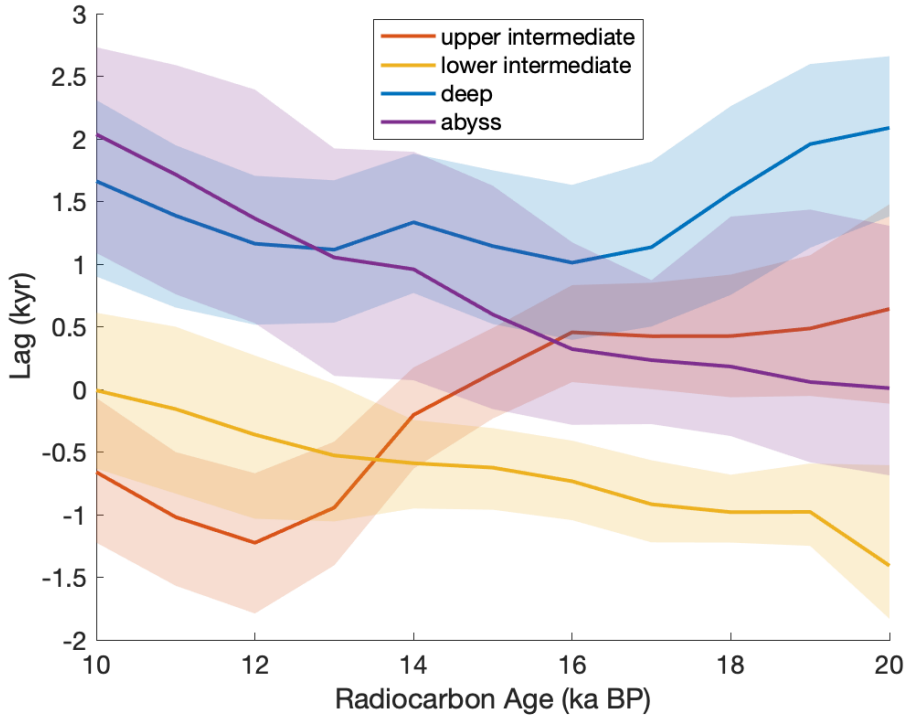

Figure 10: Stacks of lag times from 10-20 ka BP for the upper and lower intermediate, deep, and abyss groups.

References

1. Adkins, Jess F., Katherine McIntyre, and Daniel P. Schrag. "The salinity, temperature, and δ18O of the glacial deep ocean." *Science* 298, no. 5599 (2002): 1769-1773.

2. Ahn, Seonmin, Deborah Khider, Lorraine E. Lisiecki, and Charles E. Lawrence. "A probabilistic Pliocene–Pleistocene stack of benthic δ18O using a profile hidden Markov model." *Dynamics and Statistics of the Climate System* 2, no. 1 (2017).

3. Blaauw, Maarten, and J. Andrés Christen. "Flexible paleoclimate age-depth models using an autoregressive gamma process." *Bayesian analysis* 6, no. 3 (2011): 457-474.

4. Boyle, Edward A., and Lloyd Keigwin. "North Atlantic thermohaline circulation during the past 20,000 years linked to high-latitude surface temperature." *Nature* 330, no. 6143 (1987): 35.

5. Broecker, W. S., M. Andree, G. Bonani, W. Wolfli, H. Oeschger, M. Klas, A. Mix, and W. Curry. "Preliminary estimates for the radiocarbon age of deep water in the glacial ocean." *Paleoceanography* 3, no. 6 (1988): 659-669.

6. Christen, J. Andrés, and Sergio Pérez. "A new robust statistical model for radiocarbon data." *Radiocarbon* 51, no. 3 (2009): 1047-1059.

7. Cortese, Giuseppe, Andrea Abelmann, and Rainer Gersonde. "The last five glacial-interglacial transitions: A high-resolution 450,000-year record from the subantarctic Atlantic." *Paleoceanography* 22, no. 4 (2007).

8. Curry, William B., and Delia W. Oppo. "Glacial water mass geometry and the distribution of δ13C of ΣCO2 in the western Atlantic Ocean." *Paleoceanography* 20, no. 1 (2005).

9. DeVries, Tim, and François Primeau. "Dynamically and observationally constrained estimates of water-mass distributions and ages in the global ocean." *Journal of Physical Oceanography* 41, no. 12 (2011): 2381-2401.

10. Duplessy, J. C., N. J. Shackleton, R. G. Fairbanks, L. Labeyrie, D. Oppo, and N. Kallel. "Deepwater source variations during the last climatic cycle and their impact on the global deepwater circulation." *Paleoceanography* 3, no. 3 (1988): 343-360.

11. Duplessy, J. C., E. Bard, M. Arnold, N. J. Shackleton, J. Duprat, and L. Labeyrie. "How fast did the ocean—atmosphere system run during the last deglaciation?." *Earth and Planetary Science Letters* 103, no. 1-4 (1991): 27-40.

12. EPICA, Community Members. "One-to-one coupling of glacial climate variability in Greenland and Antarctica." *Nature* 444, no. 7116 (2006): 195.

13. Gebbie, G. (2012). Tracer transport timescales and the observed Atlantic-Pacific lag in the timing of the Last Termination. *Paleoceanography*, *27*(3).

14. Gebbie, Geoffrey, and Peter Huybers. "The mean age of ocean waters inferred from radiocarbon observations: Sensitivity to surface sources and accounting for mixing histories." *Journal of Physical Oceanography* 42, no. 2 (2012): 291-305.

15. Gebbie, Geoffrey. "How much did glacial North Atlantic water shoal?." *Paleoceanography* 29, no. 3 (2014): 190-209.

16. Gebbie, Geoffrey, Carlye D. Peterson, Lorraine E. Lisiecki, and Howard J. Spero. "Global-mean marine δ13C and its uncertainty in a glacial state estimate." *Quaternary Science Reviews* 125 (2015): 144-159.

17. He, Feng, Jeremy D. Shakun, Peter U. Clark, Anders E. Carlson, Zhengyu Liu, Bette L. Otto-Bliesner, and John E. Kutzbach. "Northern Hemisphere forcing of Southern Hemisphere climate during the last deglaciation." *Nature* 494, no. 7435 (2013): 81.

18. Hoffman, J. L., and D. C. Lund. "Refining the stable isotope budget for Antarctic Bottom Water: New foraminiferal data from the abyssal southwest Atlantic." *Paleoceanography and Paleoclimatology* 27, no. 1 (2012).

19. Imbrie, John, James D. Hays, Douglas G. Martinson, Andrew McIntyre, Alan C. Mix, Joseph J. Morley, Nicklas G. Pisias, Warren L. Prell, and Nicholas J. Shackleton. "The orbital theory of Pleistocene climate: support from a revised chronology of the marine d18O record." (1984).

20. Keigwin, L. D., G. A. Jones, and P. N. Froelich. "A 15,000 year paleoenvironmental record from Meiji Seamount, far northwestern Pacific." *Earth and Planetary Science Letters* 111, no. 2-4 (1992): 425-440.

21. Labeyrie, Laurent, Claire Waelbroeck, Elsa Cortijo, Elisabeth Michel, and Jean-Claude Duplessy. "Changes in deep water hydrology during the Last Deglaciation." *Comptes Rendus Geoscience* 337, no. 10-11 (2005): 919-927.

22. Lee, Taehee, Lorraine Lisiecki, Devin Rand, Charles Laurence, Jake Gebbie. "Dual Proxy Gaussian Process Stack: Integrating Benthic d18O and Radiocarbon Proxies for Inferring Ages on Ocean Sediment Cores. *In Preparation*, https://arxiv.org/abs/1907.08738

23. Lin, Luan, Deborah Khider, Lorraine E. Lisiecki, and Charles E. Lawrence. "Probabilistic sequence alignment of stratigraphic records." *Paleoceanography* 29, no. 10 (2014): 976-989.

24. Lougheed, Bryan C., and S. P. Obrochta. "A Rapid, Deterministic Age-Depth Modeling Routine for Geological Sequences With Inherent Depth Uncertainty." *Paleoceanography and Paleoclimatology* 34, no. 1 (2019): 122-133.

25. Lund, D. C., A. C. Tessin, J. L. Hoffman, and A. Schmittner. "Southwest Atlantic water mass evolution during the last deglaciation." *Paleoceanography and Paleoclimatology* 30, no. 5 (2015): 477-494.

26. Lynch-Stieglitz, Jean, Jess F. Adkins, William B. Curry, Trond Dokken, Ian R. Hall, Juan Carlos Herguera, Joël J-M. Hirschi et al. "Atlantic meridional overturning circulation during the Last Glacial Maximum." *science* 316, no. 5821 (2007): 66-69.

27. Mix, Alan C., and William F. Ruddiman. "Oxygen-Isotope Analyses and Pleistocene Ice Volumes 1." *Quaternary Research* 21, no. 1 (1984): 1-20.

28. Makou, Matthew C., Timothy I. Eglinton, Delia W. Oppo, and Konrad A. Hughen. "Postglacial changes in El Niño and la Niña behavior." *Geology* 38, no. 1 (2010): 43-46.

29. Marchitto, Thomas M., and Wallace S. Broecker. "Deep water mass geometry in the glacial Atlantic Ocean: A review of constraints from the paleonutrient proxy Cd/Ca." *Geochemistry, Geophysics, Geosystems* 7, no. 12 (2006).

30. Marchitto, T. M., W. B. Curry, J. Lynch-Stieglitz, S. P. Bryan, K. M. Cobb, and D. C. Lund. "Improved oxygen isotope temperature calibrations for cosmopolitan benthic foraminifera." *Geochimica et Cosmochimica Acta* 130 (2014): 1-11.

31. McManus, Jerry F., Roger Francois, J-M. Gherardi, Lloyd D. Keigwin, and Susan Brown-Leger. "Collapse and rapid resumption of Atlantic meridional circulation linked to deglacial climate changes." *Nature* 428, no. 6985 (2004): 834.

32. Mashiotta, Tracy A., David W. Lea, and Howard J. Spero. "Glacial–interglacial changes in Subantarctic sea surface temperature and δ18O-water using foraminiferal Mg." *Earth and Planetary Science Letters* 170, no. 4 (1999): 417-432.

33. Oppo, Delia W., William B. Curry, and Jerry F. McManus. "What do benthic δ13C and δ18O data tell us about Atlantic circulation during Heinrich Stadial 1?." *Paleoceanography* 30, no. 4 (2015): 353-368.

34. Rasmussen, Carl E., and Christopher K. I Williams. *Gaussian Processes for Machine Learning*. Cambridge, Mass. : MIT Press, 2006.

35. Riveiros, Natalia Vázquez, Claire Waelbroeck, Luke Skinner, Didier M. Roche, Jean-Claude Duplessy, and Elisabeth Michel. "Response of South Atlantic deep waters to deglacial warming during Terminations V and I." *Earth and Planetary Science Letters* 298, no. 3-4 (2010): 323-333.

36. Schmittner, A., O. A. Saenko, and A. J. Weaver. "Coupling of the hemispheres in observations and simulations of glacial climate change." *Quaternary Science Reviews* 22, no. 5-7 (2003): 659-671.

37. Shackleton, Nicholas. "Oxygen isotope analyses and Pleistocene temperatures re-assessed." *Nature* 215, no. 5096 (1967): 15.

38. Shackleton, N. J., J-C. Duplessy, M. Arnold, P. Maurice, M. A. Hall, and J. Cartlidge. "Radiocarbon age of last glacial Pacific deep water." *Nature* 335, no. 6192 (1988): 708.

39. Shackleton, Nicholas J. "The 100,000-year ice-age cycle identified and found to lag temperature, carbon dioxide, and orbital eccentricity." *Science* 289, no. 5486 (2000): 1897-1902.

40. Shakun, Jeremy D., Peter U. Clark, Feng He, Shaun A. Marcott, Alan C. Mix, Zhengyu Liu, Bette Otto-Bliesner, Andreas Schmittner, and Edouard Bard. "Global warming preceded by increasing carbon dioxide concentrations during the last deglaciation." *Nature* 484, no. 7392 (2012): 49.

41. Skinner, L. C., and N. J. Shackleton. "Rapid transient changes in northeast Atlantic deep water ventilation age across Termination I." *Paleoceanography* 19, no. 2 (2004).

42. Skinner, L. C., & Shackleton, N. J. (2005). An Atlantic lead over Pacific deep-water change across Termination I: implications for the application of the marine isotope stage stratigraphy. *Quaternary Science Reviews*, *24*(5-6), 571-580.

43. Skinner, L. C., Fallon, S., Waelbroeck, C., Michel, E., & Barker, S. (2010). Ventilation of the deep Southern Ocean and deglacial CO2 rise. *Science*, *328*(5982), 1147-1151.

44. Sortor, Rachel N., and David C. Lund. "No evidence for a deglacial intermediate water Δ14C anomaly in the SW Atlantic." *Earth and Planetary Science Letters* 310, no. 1-2 (2011): 65-72.

45. Stern, J. V., & Lisiecki, L. E. (2014). Termination 1 timing in radiocarbon-dated regional benthic δ18O stacks. *Paleoceanography*, *29*(12), 1127-1142.

46. Tessin, A. C., and D. C. Lund. "Isotopically depleted carbon in the mid-depth South Atlantic during the last deglaciation." *Paleoceanography* 28, no. 2 (2013): 296-306.

47. Thornalley, David JR, Stephen Barker, Wallace S. Broecker, Henry Elderfield, and I. Nick McCave. "The deglacial evolution of North Atlantic deep convection." *science* 331, no. 6014 (2011): 202-205.

48. Toggweiler, J. R., and David W. Lea. "Temperature differences between the hemispheres and ice age climate variability." *Paleoceanography* 25, no. 2 (2010).

49. Waelbroeck, C., L. C. Skinner, L. Labeyrie, J-C. Duplessy, E. Michel, Natalia Vazquez Riveiros, J-M. Gherardi, and F. Dewilde. "The timing of deglacial circulation changes in the Atlantic." *Paleoceanography* 26, no. 3 (2011).

50. Zarriess, Michelle, Heather Johnstone, Matthias Prange, Silke Steph, Jeroen Groeneveld, Stefan Mulitza, and Andreas Mackensen. "Bipolar seesaw in the northeastern tropical Atlantic during Heinrich stadials." *Geophysical Research Letters* 38, no. 4 (2011).

51. Zhang, Jiaxu, Zhengyu Liu, Esther C. Brady, Delia W. Oppo, Peter U. Clark, Alexandra Jahn, Shaun A. Marcott, and Keith Lindsay. "Asynchronous warming and δ18O evolution of deep Atlantic water masses during the last deglaciation." *Proceedings of the National Academy of Sciences* 114, no. 42 (2017): 11075-11080.